Analysis of Photocatalytic Reactors Employing the Photonic Efficiency and the Removal Efficiency Parameters: Degradation of Radiation Absorbing and Nonabsorbing Pollutants

Gerd Sagawe,[†] María L. Satuf,[‡] Rodolfo J. Brandi,[‡] Jan P. Muschner,[†] Christian Federer,[†] Orlando M. Alfano,*[,‡] Detlef Bahnemann,[†] and Alberto E. Cassano[‡]

Leibniz Universität Hannover, Institut für Technische Chemie, Callinstraβe 3, 30167 Hannover, Germany, and INTEC (Universidad Nacional del Litoral and CONICET), CCT CONICET-Edificio INTEC I, Colectora de la Ruta Nacional No. 168, km 472.5, 3000 Santa Fe, Argentina

The photocatalytic degradation of radiation absorbing and nonabsorbing pollutants in slurry reactors is analyzed in terms of two performance parameters: the *observed photonic efficiency* (OPE) and the *removal efficiency* (RE) [Sagawe et al. *Chem. Eng. Sci.* **2003**, 58, 2587]. The OPE proposal permits a simple approach to analyze complex reacting systems. Conversely, to calculate the RE, the modeling of radiation absorption and scattering inside the reactors is necessary, which requires the determination of the optical properties of the catalyst and the modeling of the optical effects of the reactor walls. The degradation of dichloroacetic acid, phenol, and 4-nitrophenol was studied employing aeroxide TiO_2 P25 from Evonik-Degussa in well-mixed batch reactors irradiated by UV lamps. 4-Nitrophenol has the particular characteristic to compete with titania for the absorption of photons in the employed wavelength range of irradiation. Two reaction kinetics proposals were considered to interpret experimental data: a "photocatalytic" Langmuir−Hinshelwood model (the L-H_{Ph} model) and a "photocatalytic" Langmuir−Hinshelwood linear model (the L-H_{Ph}/1 model). The good agreement observed between experimental results and model simulations confirms the usefulness of the proposed OPE approximation and the more accurate information provided by the RE performance parameter. The inclusion of 4-nitrophenol allowed inference of the situation that would be encountered when treating real samples contaminated with strong radiation absorbing compounds.

1. Introduction

Research on water detoxification methods has become an area of great interest due to the enduring pollution of water streams along with the enactment of increasingly stringent environmental regulations.

In the last decades, new methods characterized by the absence of selectivity and advantageous destructive outcomes have given rise to a group of alternative processes comprised under the generic name advanced oxidation technologies. One of the methods most widely studied is photocatalysis, using in the majority of the applications titanium dioxide (TiO_2) and radiation within the 300−390 nm wavelength range.

Photocatalysis with TiO_2 has proved to be an effective technology to degrade organic pollutants that are resistant to conventional air and water treatment methods. It is based on the absorption of UV radiation by the catalyst and the resulting generation of powerful oxidation species that can destroy organic matter adsorbed at the surface of TiO_2 particles.[1]

The modeling of photocatalytic reactors is a valuable tool to compare the performance of different devices, it helps to find optimal conditions for pollutant degradation, and it is fundamental for scaling-up purposes.[2−8] In this sense, the correct evaluation of the incident radiation and radiation absorption by the reacting mixture is crucial. However, the mathematical derivation of rigorous kinetic models can be complicated when working with real effluents. It is not a surprise that most of the existing rigorous publications employ model compounds that, in most cases, cannot be readily compared with empirical and well-documented studies on real mixtures of pollutants. This latter type of analysis, although useful, is not amenable of safe and inexpensive scaling up methods because of its lack of generality. Resorting to a kind of intermediate approach, a proposal was made by Sagawe et al.[9] that, properly expanded, could help to bridge the gap between accurate generalization and usefulness.

In the present work, we propose simple kinetic expressions with applicability to a large family of compounds. The chosen model pollutants were dichloroacetic acid (DCA), phenol, and 4-nitrophenol (4-NP). The case of the last compound is particularly interesting because it absorbs radiation in the wavelength range of absorption by the catalyst, adding complexity to the analysis. The influence of different operational parameters on the photocatalytic degradation of the pollutants was studied: initial pollutant concentration, catalyst concentration, radiation intensity, and reactor depth.

The photocatalytic process was evaluated by using a simple concept: the photon demand,[9] that can be employed to calculate two performance parameters: the *observed photonic efficiency* (OPE) and the *removal efficiency* (RE). These parameters relate the rate of removal of the pollutants with the rate of incident radiation (OPE) and with the rate of radiation absorption by the catalyst (RE). The evaluation of the incident radiation flux was obtained experimentally with a calibrated radiometer. The rate of radiation absorption was computed by applying a one-dimensional−one-directional radiation model[10] to the reaction space. Experiments were carried out in laboratory scale, employing a novel arrangement of slurry batch reactors with plane parallel walls. Special consideration has been given to

* To whom correspondence should be addressed. E-mail: alfano@intec.unl.edu.ar. Phone: +54-342-4511546. Fax: +54-342-4511087.
[†] Leibniz Universität Hannover.
[‡] INTEC (Universidad Nacional del Litoral and CONICET).

10.1021/ie901753k
Published on Web 03/10/2010

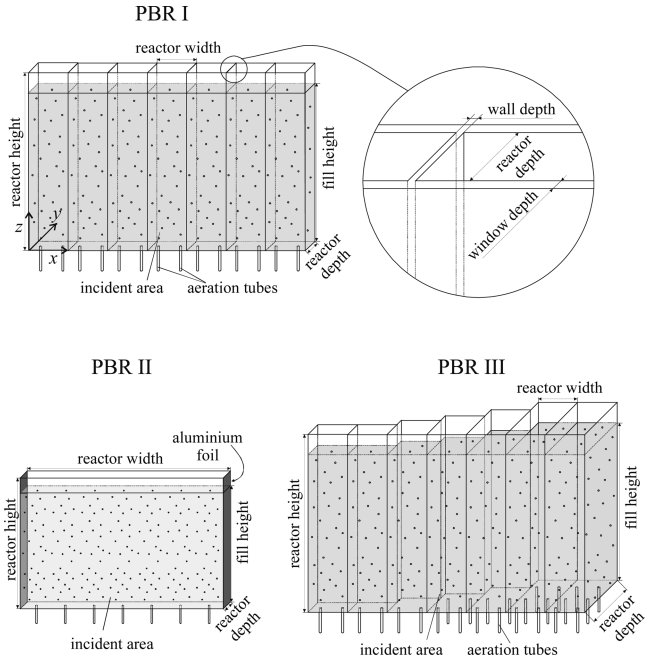

Figure 1. Schematic representation of the photocatalytic batch reactors (PBR).

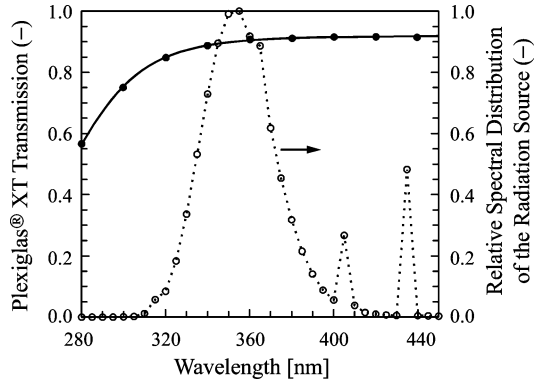

Figure 2. Optical characteristics of the reactor walls (—) and relative spectral distribution of the radiation source power output (••••).

the effects produced by the reactor walls on the radiation field in the photocatalytic reaction space.

2. Experimental Section

Chemicals. Model pollutants, DCA, phenol, and 4-NP, were of analytical grade. Titanium dioxide, aeroxide TiO_2 P25 from Evonik-Degussa, was used in the whole study (≈75% anatase/rutile) having a specific surface area of approximately 50 m^2 g^{-1} and a size of the elementary particles between 30 and 50 nm. All experiments were carried out using distilled and deionized water (Milli-Q water, 18 MΩ cm).

Reactors. Three types of photocatalytic batch reactors (PBR), illustrated in Figure 1, were employed in the present study. They are made of a special, commercial Plexiglas XT (polymethylmethacrylate) from Röhm GmbH, transparent to radiation at almost all wavelengths in the UV-A range as shown in Figure 2 (absorption becomes significant at shorter wavelengths). Air injection nozzles (Compressor ME 2C Vacuubrand GmbH & Co.) located at the bottom of the reactors provide variable oxygen concentration throughout the experiments (very often constant and ca. 8 mg L^{-1}), good catalyst distribution, and efficient mixing conditions. The reactors were designed to obtain almost homogeneous incoming radiation flux at the front windows. Dimensions of the PBR are presented in Table 1.

Table 1. Dimensions of the Photocatalytic Batch Reactors (PBR)

type	width (mm)	depth (mm)	height (mm)
PBR Ia	30	12.0	400
PBR Ib	60	12.8	400
PBR II	200	4/6/9/12	220
PBR III	60	20/35/50/75/100	320

PBRs Ia and Ib consist of two acrylic walls divided into individual chambers by transversely located double acrylic sheets. This type of reactor allows one to carry out simultaneously different experiments under identical reactor operating conditions. The dividing walls are transparent and relatively thin (2 mm width). Therefore, they can divide the reaction space into individual reactor elements without sensibly altering the homogeneity of the radiation field in the plane parallel to the radiation entrance wall ($x-z$ plane in Figure 1). A reactor element employed for kinetic analysis must be located between two other reactor elements filled with a suspension of equal, or at least very similar, optical properties in order to avoid the nonhomogeneities of the radiation field on the lateral walls. PBRs Ia and Ib differ mainly in the width of the individual reactors and only slightly in their depth (see Table 1).

Four photoreactors of the type PBR II with different depths were constructed. To reduce to negligible values the interference of the lateral walls on the radiation field, they were covered with adhesive aluminum foil.

PBR III varies from PBR Ib only in the different depths of the individual reactors.

The transmission of the reactor walls was regularly measured to evaluate the influence of the catalyst particles adherence to them. The titanium dioxide sticking to the acrylic walls during the experiments was negligible. In the wavelength range of 300−390 nm, this is a significant advantage with respect to reactors made of borosilicate glass.

Radiation Emitting Device. Sixteen UV-A lamps (CLEO R Performance, 40 W each, from Philips having a lamp length of 600 mm) were horizontally placed inside a box. The front side of the box was covered with a light diffuser to obtain homogeneous and almost isotropic radiation at the reactor windows. The diffuser consists of a grounded acrylic sheet (Plexiglas XT). In addition, an aluminum reflector was placed at the borders of the lamp box. The radiation emitting area was 700 mm × 400 mm. The wavelength emission range of the lamps was 300−420 nm, with a peak near 350 nm, as shown in Figure 2. The incident radiation flux at the reactor windows ($q_{inc}^{\Delta\lambda}$) at the beginning of each experiment, was measured with an UV-A radiometer (Nr 1548 from Dr. Hönle UV-Technik). The instrument was subjected to an accurate calibration procedure, particularly regarding its spectral wavelength sensitivity.

Procedure. The aqueous TiO_2 suspensions were magnetically stirred during 30 min before the beginning of the experiments. The initial pH of the suspension containing DCA was fixed at 4 with either NaOH or H_2SO_4. KNO_3 was added to increment the conductivity of the reacting mixture (10 mmol L^{-1}). During the degradation of DCA, the pH of the suspension decreases due to the liberation of H^+ cations, reaching values between 2 and 3, depending on the initial concentration of DCA. When phenol and 4-NP were employed as model substances, the pH of the suspensions was adjusted at pH = 3 with NaOH or HCl. The experiments were carried out at ambient conditions of temperature and pressure (20 °C and 1.0 × 10^5 Pa, respectively). Samples were regularly withdrawn from the reactors and

centrifuged to remove the catalyst particles before analysis. The volume of the samples ranged from 5 to 10 mL.

Chemical Analysis. The concentration of phenol and 4-NP was measured by HPLC analysis employing a Dionex chromatograph (Series 4500i) equipped with a C18 reversed phase column (NUCLEOSIL 100-10 C18 250/4 ET) and a UV detector (Dionex Variable Wavelength Detector, Series 4500i). The eluent consisted of a mixture of methanol (49.5%), water (49.5%), and acetic acid (1%), pumped at a rate of 1.5 mL min^{-1}. The detection wavelength was 270 nm.

The final products of the photocatalytic degradation of DCA are HCl and CO_2. As there are no stable intermediates formed during this reaction,[11−13] each mole of DCA releases 2 mol Cl^-. Therefore, the concentration of DCA was indirectly assessed by quantification of chloride ions employing a selective membrane electrode (Nr 6.0502.120, Metrohm) that was precisely calibrated for this particular reaction system. The pH of the reacting mixture was measured also online with a Metrohm pH-meter (Type 691).

Mineralization of the pollutants was assessed by total organic carbon (TOC) analysis, employing a Shimadzu TOC-5000 A analyzer. It was particularly useful to detect the existence of reaction intermediates when working with phenol and 4-NP.

The optical properties of the catalyst and pollutants suspensions were measured with a Cary 5 UV/vis-NIR spectrophotometer (Varian). For aeroxide TiO_2 P25, the instrument was equipped with an Ulbricht integrating sphere, and the properties were obtained employing a slight modification of the method published by Satuf et al.[14] They comprise the spectral specific (per unit mass concentration) absorption (κ_λ^*), scattering (σ_λ^*), and extinction ($\beta_\lambda^* = \kappa_\lambda^* + \sigma_\lambda^*$) coefficients and the asymmetry factor (g_λ) of the adopted phase function for scattering, corresponding to the Henyey and Greenstein model.[15] More details are given in section 3.5.

3. Theoretical

3.1. Observed Photonic Efficiency (OPE) and Removal Efficiency (RE). The actual observed photonic efficiency (actual OPE) has been defined as[9]

$$\zeta_{act}^{obs} = \frac{\text{rate of substance removal from the liquid}}{\text{rate of incident photons}} = \frac{dN_{rem}/dt}{dP_{inc}^{\Delta\lambda}/dt} \quad (1)$$

where

$$dP_{inc}^{\Delta\lambda}/dt = \langle q_{inc}^{\Delta\lambda}\rangle_{A_{inc}} A_{inc} = \int_{A_{inc}} q_{inc}^{\Delta\lambda}(\underline{x}, t)\, dA = \int_{A_{inc}} dA \int_{\lambda_1}^{\lambda_2} d\lambda \int_{\Omega_{inc}} I_{\Omega,\lambda}(\underline{x}, t)\underline{\Omega}\cdot\underline{n}\, d\Omega \quad (2)$$

This property can be calculated based on directly "observable" variables. It is clear that it does not have the accuracy of a properly defined quantum yield, but it is very simple to measure and calculate.

The actual OPE can be rewritten as

$$\zeta_{act}^{obs} = \frac{\langle (dC/dt)_{rem}\rangle_{V_{Sys,L}} V_{Sys,L}}{\langle q_{inc}^{\Delta\lambda}\rangle_{A_{inc}} A_{inc}} \quad (3)$$

It is worth noticing that the amount of substance removed from the liquid includes that part of the substance adsorbed on the catalytic particles; i.e., not only the mass of pollutant that has reacted but also the one that has been physically removed from the liquid.

Besides, the removal efficiency (RE) has been defined as[9]

$$\eta_{remov} = \frac{\text{rate of substance removal from the liquid}}{\text{rate of photon absorption by the catalyst}} = \frac{\langle (dC/dt)_{rem}\rangle_{V_{Sys,L}} V_{Sys,L}}{\langle e_{abs}^{\Delta\lambda}\rangle_{V_{Sys}} V_{Sys}} \quad (4)$$

The RE is equivalent to a polychromatic quantum yield.

Considering eqs 3 and 4, we can express

$$\zeta_{act}^{obs} = \vartheta_{cat}\eta_{remov} \quad (5)$$

where ϑ_{cat} is the overall catalyst absorption efficiency, defined as

$$\vartheta_{cat} = \frac{\text{rate of photon absorption by the catalyst}}{\text{rate of incident photons at the reactor wall}} = \frac{\langle e_{abs}^{\Delta\lambda}\rangle_{V_{Sys}} V_{Sys}}{\langle q_{inc}^{\Delta\lambda}\rangle_{A_{inc}} A_{inc}} \quad (6)$$

3.2. Mass Balance for PBR. The mass balance for a batch reactor, assuming isothermal and perfectly mixed conditions, can be written as[9]

$$\varepsilon_L V_{Sys} \frac{d\langle C_i\rangle_{V_{Sys,L}}}{dt} = -\langle (dC_i/dt)_{rem}\rangle_{V_{Sys,L}} V_{Sys,L} \quad (7)$$

Introducing the OPE concept (eq 3), results in

$$\varepsilon_L V_{Sys} \frac{d\langle C_i\rangle_{V_{Sys,L}}}{dt} = -\zeta_{act}^{obs}\langle q_{inc}^{\Delta\lambda}\rangle_{A_{inc}} A_{inc} \quad (8)$$

From now on, to simplify notation, the average symbol ⟨⟩ will be omitted. Hence, C_i indicates volume averaged concentration, and $q_{inc}^{\Delta\lambda}$ is the incident radiation flux averaged over the reactor incident area.

The actual OPE can be described as a function of the initial conditions of the process (ψ^0), of the actual relative concentration of the target compound (C_i/C_i^0), and of the actual photon flux ($q_{inc}^{\Delta\lambda}$). In addition, if we define the reference OPE ($\zeta^\otimes$) as the OPE obtained at a reference photon flux $q_{inc}^{\Delta\lambda,\otimes}$, ζ_{act}^{obs} can be written as

$$\zeta_{act}^{obs} = \zeta^\otimes(\psi^0, C_i/C_i^0, q_{inc}^{\Delta\lambda,\otimes}) \times f_q(q_{inc}^{\Delta\lambda}/q_{inc}^{\Delta\lambda,\otimes}) \quad (9)$$

The reference photon flux must be defined at any arbitrary but fixed condition, i.e., independent of time. The function f_q accounts for the deviations of the actual photon flux from the reference photon flux. For low irradiation rates, the OPE is independent of the photon flux[9] and the function f_q is equal to 1. Due to the experimental conditions employed in the present work, it is safe to assume that in a first instance $f_q = 1$.

Introducing eq 9 into eq 8 and integrating over the reaction time renders

$$-\int_{C_i^0}^{C_i} \frac{dC_i'}{\zeta^\otimes(\psi^0, C_i'/C_i^0)} = \frac{A_{inc}}{\varepsilon_L V_{Sys}} \int_0^t q_{inc}^{\Delta\lambda}\, dt' \quad (10)$$

The left-hand side of the above equation represents the *photon demand* per unit liquid volume that is required by the system to change from C_i^0 to C_i when the system is irradiated with $q_{inc}^{\Delta\lambda,\otimes}$

$$\mathrm{PD}^{\otimes} = -\int_{C_i^0}^{C_i} \frac{\mathrm{d}C_i'}{\zeta^{\otimes}(\psi^0, C_i'/C_i^0)} \tag{11}$$

3.3. L-H_{Ph} Kinetics for DCA. The photocatalytic degradation of DCA can be well-described employing so-called Langmuir−Hinshelwood (L-H) kinetics.[9] By adapting the L-H equation to the OPE concept (L-H_{Ph}), we can employ the following empirical expression

$$\zeta^{\otimes}(C_i) = \zeta_{\max}^{\otimes} \frac{KC_i}{1 + KC_i} \tag{12}$$

where $\zeta_{\max}^{\otimes}$ is the reference OPE at high substrate concentrations.

According to eq 11, the reference photon demand corresponding to the L-H_{Ph} kinetics is (see Table 1 in the work of Sagawe et al.[9])

$$\mathrm{PD}^{\otimes} = -\frac{C_i^0}{\zeta_{\max}^{\otimes}} \frac{1}{KC_i^0} \left[\ln\left(\frac{C_i}{C_i^0}\right) - KC_i^0 \left(1 - \frac{C_i}{C_i^0}\right) \right] \tag{13}$$

Assuming that $q_{\mathrm{inc}}^{\Delta\lambda}$ remains constant throughout the reaction time, as it is the case in the laboratory experiments, and expressing $\zeta_{\max}^{\otimes} = \vartheta_{\mathrm{cat}} \eta_{\max}^{\otimes}$, we obtain the following equation representing the mass balance for DCA:

$$-\left[\ln\left(\frac{C_i}{C_i^0}\right) - KC_i^0 \left(1 - \frac{C_i}{C_i^0}\right) \right] = KC_i^0 \frac{\vartheta_{\mathrm{cat}} \eta_{\max}^{\otimes}}{C_i^0} \frac{A_{\mathrm{inc}}}{\varepsilon_{\mathrm{L}} V_{\mathrm{Sys}}} q_{\mathrm{inc}}^{\Delta\lambda} t \tag{14}$$

If the parameters K and $\eta_{\max}^{\otimes}$ are known, the DCA concentration C_i can be calculated iteratively as a function of time, knowing also the process parameters ε_{L}, V_{Sys}, A_{inc}, $q_{\mathrm{inc}}^{\Delta\lambda}$, C_i^0, and ϑ_{cat}. The kinetic parameters K and $\eta_{\max}^{\otimes}$ can be obtained by complying with the following steps:

(i) Calculation of the initial reference OPE $\zeta_0^{\otimes}$: At the beginning of the reaction, for high substrate concentrations, the L-H_{Ph} kinetics can be approximated by zero-order kinetics, with the resulting expressions for $\zeta^{\otimes}$ and $\mathrm{PD}^{\otimes}$:

$$\zeta^{\otimes} = \zeta_{\max}^{\otimes} \tag{15}$$

$$\mathrm{PD}^{\otimes} = \frac{C_i^0}{\zeta_{\max}^{\otimes}} \left(1 - \frac{C_i}{C_i^0}\right) \tag{16}$$

Then, $\zeta_0^{\otimes}$ can be calculated from the initial slope of the plot C_i/C_i^0 vs time:

$$\frac{C_i}{C_i^0} = 1 - \frac{\zeta_0^{\otimes}}{C_i^0} \frac{A_{\mathrm{inc}}}{\varepsilon_{\mathrm{L}} V_{\mathrm{Sys}}} q_{\mathrm{inc}}^{\Delta\lambda} t \tag{17}$$

(ii) Plotting of the reciprocal values of the initial removal efficiency ($1/\eta_0^{\otimes} = \vartheta_{\mathrm{cat}}/\zeta_0^{\otimes}$) vs the reciprocal values of the initial concentration ($1/C_i^0$). In case of a linear dependence, the parameters K and $\eta_{\max}^{\otimes}$ can be calculated from the slope and the intercept of the plot

$$\frac{1}{\eta_0^{\otimes}} = \frac{\vartheta_{\mathrm{cat}}}{\zeta_0^{\otimes}} = \frac{1}{\eta_{\max}^{\otimes}} + \frac{1}{\eta_{\max}^{\otimes} K} \frac{1}{C_i^0} \tag{18}$$

The above expression is obtained by transformation of eq 12 and by considering

$$\zeta_0^{\otimes} = \vartheta_{\mathrm{cat}} \eta_0^{\otimes} \quad \text{and} \quad \zeta_{\max}^{\otimes} = \vartheta_{\mathrm{cat}} \eta_{\max}^{\otimes}$$

3.4. L-H_{Ph}/1 Kinetics for Phenol and 4-NP. The term L-H_{Ph}/1 kinetics refers to a combination of initial L-H kinetics followed by first-order kinetics[9,16,17]

$$\zeta^{\otimes}(C_i) = \zeta_{\max}^{\otimes} \frac{KC_i^0}{1 + KC_i^0} \frac{C_i}{C_i^0} \tag{19}$$

The reference photon demand corresponding to the L-H_{Ph}/1 kinetics is (see Table 1 in the work of Sagawe et al.[9])

$$\mathrm{PD}^{\otimes} = -\left(\frac{1 + KC_i^0}{KC_i^0}\right) \frac{C_i^0}{\zeta_{\max}^{\otimes}} \ln\left(\frac{C_i}{C_i^0}\right) \tag{20}$$

Then, the mass balance equation for phenol and 4-NP can be expressed as

$$\ln\left(\frac{C_i}{C_i^0}\right) = -\frac{\vartheta_{\mathrm{cat}} \eta_{\max}^{\otimes}}{C_i^0} \frac{KC_i^0}{1 + KC_i^0} \frac{A_{\mathrm{inc}}}{\varepsilon_{\mathrm{L}} V_{\mathrm{Sys}}} q_{\mathrm{inc}}^{\Delta\lambda} t \tag{21}$$

The kinetic parameters K and $\eta_{\max}^{\otimes}$ can be computed as follows:

(i) Calculation of the initial reference OPE: $\zeta_0^{\otimes}$ can be obtained from the slope of the plot $\ln(C_i/C_i^0)$ vs time, with

$$\zeta_0^{\otimes} = \vartheta_{\mathrm{cat}} \eta_{\max}^{\otimes} \frac{KC_i^0}{1 + KC_i^0}$$

(ii) As in the case of DCA, the parameters K and $\eta_{\max}^{\otimes}$ can be calculated from the slope and the intercept of a plot constructed with the same method as described for eq 18.

3.5. Radiation Model. Radiative Transfer Equation (RTE) for a One-Dimensional−One-Directional Model. The rate of photon absorption by the catalyst is required to compute the value of ϑ_{cat}, as shown in eq 6. Because of the design characteristics of the experimental device (reactor dimensions and diffuse incoming radiation), the reactors can be modeled as plane-parallel systems with azimuthal symmetry.[10,18] The radiation model considers that (i) the radiation arriving at the reactors windows ($x-z$ plane in Figure 1) is uniform, (ii) the main changes in the radiation spatial distribution occur along the y coordinate axis, due to the significant extinction produced by the catalyst particles, and (iii) the arrangement of the lamps, diffuser plate, and reflector ensures the arrival of diffuse radiation with azimuthal symmetry at the reactor windows. Under the former assumptions, a one-dimensional (y in space), one-directional (θ in the direction of the photon beams propagation) radiation transport model was applied to solve the RTE in the PBR:

$$\mu \frac{\partial I_\lambda(y,\mu)}{\partial y} + \beta_\lambda I_\lambda(y,\mu) = \frac{\sigma_\lambda}{2} \int_{\mu'=-1}^{1} I_\lambda(y,\mu') p(\mu,\mu') \, \mathrm{d}\mu' \tag{22}$$

where $\mu = \cos\theta$. The spectral, linear, Napierian extinction coefficient, β_λ, is defined as the sum of the spectral, linear, Napierian absorption and scattering coefficients ($\beta_\lambda = \kappa_\lambda + \sigma_\lambda$). The phase function $p(\mu, \mu')$ represents the probability that the incident radiation from direction μ' will be scattered and incorporated into the direction μ.

The phase function adopted in this study corresponds to the Henyey and Greenstein model, represented by[15]

$$p_{\mathrm{HG},\lambda}(\mu^*) = \frac{(1 - g_\lambda{}^2)}{(1 + g_\lambda{}^2 - 2g_\lambda \mu^*)^{3/2}} \tag{23}$$

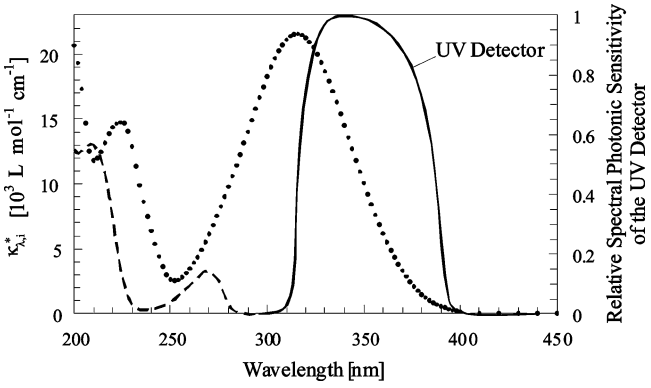

Figure 3. Spectral Napierian molar absorption coefficients of phenol (- - -) and 4-NP (····) and spectral relative photonic sensitivity of the UV detector (—).

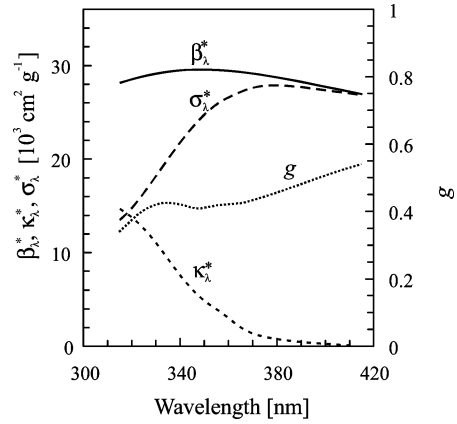

Figure 4. Catalyst optical properties as a function of wavelength: κ_λ^* spectral specific absorption coefficient; σ_λ^* spectral specific scattering coefficient; β_λ^* spectral specific extinction coefficient; g_λ asymmetry factor of the employed phase function.

where g_λ is the asymmetry factor and μ^* is the cosine of the angle formed by the incident and scattered rays.

Radiation coming from the lamps travels along five media: air, front acrylic window, reacting suspension, back acrylic window, and air; i.e., a ray crosses four interfaces. Hence, the RTE was solved inside the front window plate, in the reaction space, and inside the back window plate. The acrylic plates do not scatter radiation ($\sigma_\lambda = 0$) but present a slight absorption, mainly at short wavelengths (see Figure 2). Conversely, in the reaction space, absorption and scattering take place. The boundary conditions of the RTE at each media take into account the optical phenomena of refraction and reflection. A detailed description of the equations involved in the radiation model are presented in the Appendix.

Optical Properties. The spectral, linear, Napierian molar absorption coefficients ($\kappa_{\lambda,i}^*$) of the model pollutants DCA, phenol, and 4-NP were calculated by standard absorption measurements employing a Lambda 17 UV−vis spectrophotometer (Perkin-Elmer). Results for phenol and 4-NP are depicted in Figure 3. Additionally, the relative spectral photonic sensitivity of the UV detector as a function of wavelength is shown in the figure. The absorption of DCA (not shown) and phenol is negligible for wavelengths above 300 nm. In addition, the photocatalytic degradation products of these pollutants do not absorb radiation beyond 300 nm. On the contrary, 4-NP strongly absorbs in the wavelength region of the emission by the lamps. A study of the absorption spectra during the photocatalytic degradation of 4-NP has shown that the initial absorption of the solution only changes appreciably when conversion of the model pollutant exceeds 90%. This effect can be attributed to the fact that the absorption spectra of the reaction intermediates are similar to that of the original compound. Consequently, in the present work, the absorption of 4-NP solutions is considered to remain constant along the reaction time until 90% conversion is obtained.

The optical parameters of the catalyst suspensions β_λ^*, σ_λ^*, and κ_λ^* and the asymmetry factor g_λ for aeroxide TiO_2 P25 were calculated following a similar procedure to the one described in Satuf et al.[14] The methodology involves diffuse reflectance and transmittance spectrophotometric measurements of TiO_2 suspensions (employing an Ulbricht integrating sphere attachment), the evaluation of the radiation field in the spectrophotometer sample cell, and the application of a nonlinear optimization program to adjust the model predictions to the experimental data. The results are presented in Figure 4. The obtained values for g_λ indicates a predominant forwardly directed scattering by the catalytic particles.

The discrete ordinate method[19] was applied to solve the radiation model. This method transforms the RTE into a discrete set of equations that can be solved numerically. The solution of the RTE provides the values of $I_\lambda(y, \mu)$ at each point y and each direction μ inside the reactor, for each wavelength λ of interest. The volume-averaged rate of photon absorption in the wavelength range of emission by the lamps is calculated from the values of $I_\lambda(y, \mu)$ as

$$\langle e_{\text{abs}}^{\Delta\lambda} \rangle_{V_{\text{Sys}}} = \frac{2\pi}{V_{\text{Sys}}} \int_{V_{\text{Sys}}} \int_{\lambda_1}^{\lambda_2} \kappa_\lambda \int_{\mu=-1}^{1} I_\lambda(y,\mu)\, \mathrm{d}\mu\, \mathrm{d}\lambda\, \mathrm{d}V \quad (24)$$

4. Results and Discussion

4.1. Radiation Description. The radiation model results were experimentally validated in a PBR II with a depth (d_{PR}) of 12 mm (Table 1). The transmitted and reflected radiation fluxes measured with the calibrated UV-A detector were compared with the corresponding values provided by the complete one-dimensional−one-directional model. Different concentrations of aeroxide TiO_2 P25 (C_{cat}) were assayed. The results in terms of relative transmitted ($0 \le R_{\text{Trans}} \le 1$) and reflected ($0 \le R_{\text{Ref}} \le 1$) radiation as a function of the catalyst concentration, without and with the addition of 0.1 mmol L^{-1} of 4-NP are shown in Figure 5a and b, respectively.

The catalyst absorption efficiency ϑ_{cat} for a suspension of 5.0 g L^{-1} of aeroxide TiO_2 P25 as a function of the pollutants concentration is shown in Figure 6. As expected, neither DCA nor phenol affects the value of ϑ_{cat} because they do not absorb radiation in the UV-A range. On the contrary, increasing the concentration of 4-NP significantly diminishes the value of ϑ_{cat}, acting as an inner filtering of radiation and reducing the availability of photons for the photocatalytic reaction.

The optical thickness τ at the maximum lamp emission wavelength (350 nm) can be defined as $\tau = \beta_{350\text{nm}}^* d_{\text{PR}} C_{\text{cat}}$. This parameter allows one to compare the performance of photocatalytic reactors with different catalyst concentrations and different reactor depths. Figure 7a reports the absorption efficiency of aeroxide TiO_2 P25 as a function of the catalyst concentration (bottom x-axis) and τ (top x-axis) for different pollutants concentrations, and $d_{\text{PR}} = 12$ mm. In the absence of UV-A absorbing species, ϑ_{cat} reaches its maximum value of 0.676 even at a relatively low TiO_2 concentration of 0.5 g L^{-1}

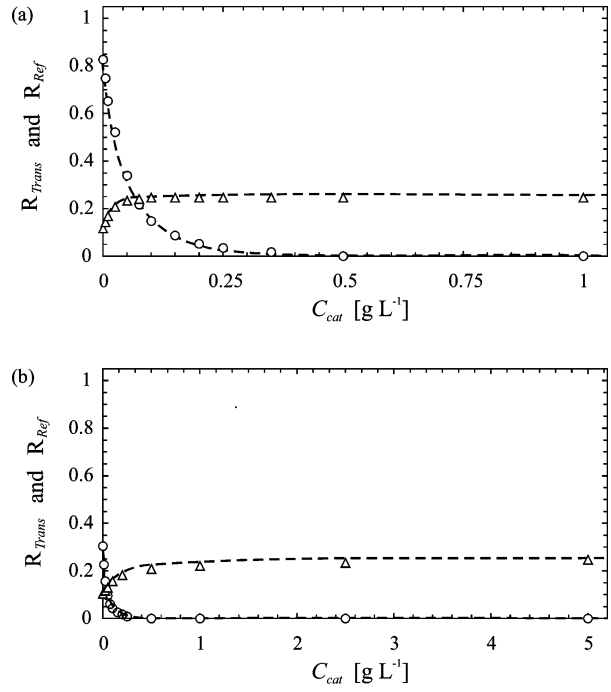

Figure 5. Experimental and calculated transmited and reflected radiation as a function of the catalyst concentration. PBR II. d_{PR} = 12 mm. (a) Aeroxide TiO_2 P25 alone. (b) Aeroxide TiO_2 P25 with 0.1 mmol L^{-1} of 4-NP: (○) experimental R_{Trans}, (△) experimental R_{Ref}, (- - -) model predictions.

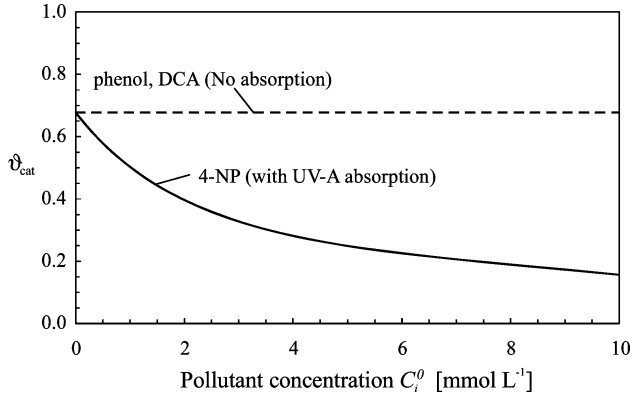

Figure 6. Catalyst absorption efficiency ϑ_{cat} as a function of the pollutants concentration. PBR II. d_{PR} = 12 mm. C_{cat} = 5.0 g L^{-1}.

(τ = 18). With the addition of 4-NP, the maximum absorption efficiency is obtained at higher catalyst concentrations. In the presence of 1.0 mmol L^{-1} of 4-NP, only 90% of the maximum value can be obtained at very high TiO_2 concentrations (C_{cat} = 15.0 g L^{-1}). These results clearly show that samples containing radiation absorbing species require high catalyst concentrations to reach significant absorption levels by the semiconductor. The catalyst absorption efficiency as a function of the reactor depth is illustrated in Figure 7b, for C_{cat} = 0.25 g L^{-1}. ϑ_{cat} increases with the reactor depth until it reaches a maximum, but this value is clearly lower when the concentration of 4-NP augments. We can conclude that, in the absence of absorbing species, the maximum ϑ_{cat} can be obtained by increasing either the catalyst loading or the reactor depth. However, when radiation absorbing species are present, this is only achievable by increasing the catalyst concentration.

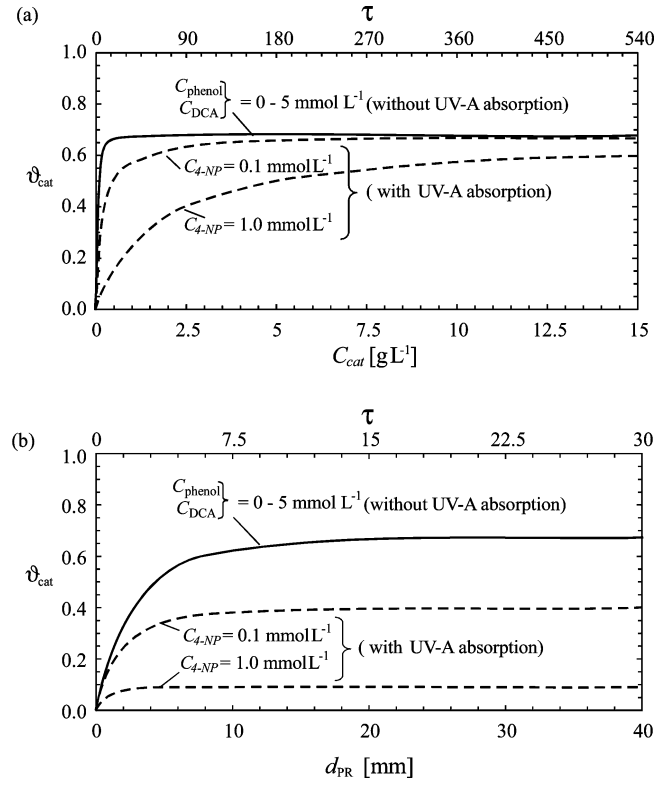

Figure 7. (a) Catalyst absorption efficiency ϑ_{cat} as a function of the catalyst concentration and the optical thickness, for different pollutants concentrations. PBR II. d_{PR} = 12 mm. (b) Catalyst absorption efficiency ϑ_{cat} as a function of the reactor depth and the optical thickness, for different pollutants concentrations. C_{cat} = 0.25 g L^{-1}.

4.2. Kinetic Results. Adsorption of the model compounds on the catalyst particles was negligible under our experimental conditions (less than 3% of the initial pollutant concentration). Consequently, the values of the observed photonic efficiency correspond to the values of conventional photonic efficiency.

Model Pollutant: DCA. All experiments with DCA were carried out in a PBR Ib.

(a) Influence of the Initial Pollutant Concentration. Experiments with different initial DCA concentrations (C_i^0) were performed to study the influence of the pollutant concentration on the OPE. The concentration of aeroxide TiO_2 P25 was fixed at 5.0 g L^{-1} for all experiments. As illustrated in Figure 8a, the photocatalytic degradation of DCA can be accurately represented by the L-H_{Ph} kinetics (eq 14) with the parameters K and $\eta^{\otimes}_{max}$ computed as described in the theoretical section. ϑ_{cat} was obtained from the radiation model. The process parameters are the following: K = 1.07 L mmol^{-1}; $\eta^{\otimes}_{max}$ = 0.189; ϑ_{cat} = 0.676; $q^{\Delta\lambda}_{inc}$ = 7.07 × 10^{-5} Einstein m^{-2} s^{-1}; $A_{inc}/(\varepsilon_L V_{Sys})$ = 83.2 m^{-1}.

Figure 8b depicts the experimental and model values of the reference initial OPE $\zeta_0^{\otimes}$ and the reference initial removal efficiency $\eta_0^{\otimes}$ as a function of the initial DCA concentration. The inset represents the plot $1/\eta_0^{\otimes}$ vs $1/C_i^0$ and the fitting equation to obtain the parameters K and $\eta^{\otimes}_{max}$. The estimated values of $\zeta_0^{\otimes}$ and $\eta_0^{\otimes}$ were calculated according to eqs 12 and 5, respectively. As observed in Figure 8b, $\zeta_0^{\otimes}$ and $\eta_0^{\otimes}$ are predicted with good accuracy by the L-H_{Ph} kinetics. They increase with the initial DCA concentration until reaching a maximum value at high C_i^0.

A comparison between the values of photonic efficiency obtained in the present work with the ones reported in the literature is not straightforward because variations in the experimental conditions, reactor geometries, or type of lamps

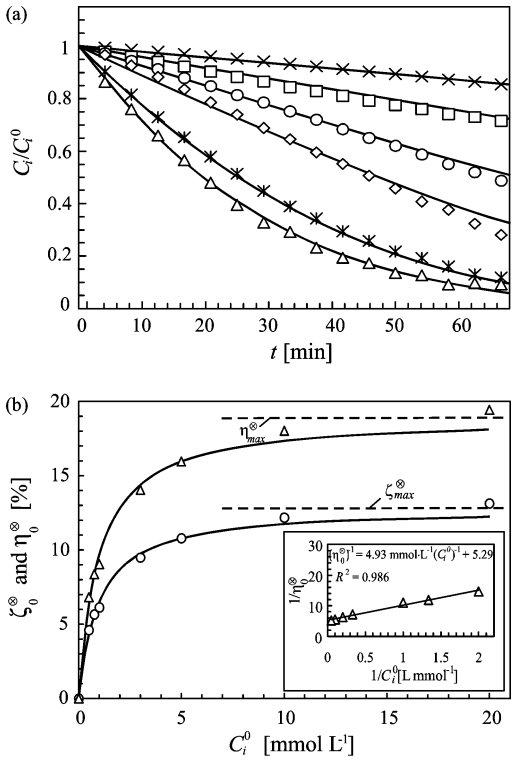

Figure 8. (a) Dimensionless DCA concentration vs time for different initial pollutant concentrations. Symbols: experimental data. Solid lines: model predictions. PBR Ib. $d_{PR} = 12.8$ mm. $C_{cat} = 5.0$ g L^{-1}. (×) $C_i^0 = 20$ mmol L^{-1}, (□) $C_i^0 = 10$ mmol L^{-1}, (○) $C_i^0 = 5$ mmol L^{-1}, (◇) $C_i^0 = 3$ mmol L^{-1}, (∗) $C_i^0 = 1$ mmol L^{-1}, (△) $C_i^0 = 0.5$ mmol L^{-1}. (b) Reference initial OPE $\zeta_0^{\otimes}$ and reference initial removal efficiency $\eta_0^{\otimes}$ as a function of the initial DCA concentration. Symbols: experimental data. Solid lines: model predictions. (△) $\eta_0^{\otimes}$, (○) $\zeta_0^{\otimes}$. (inset) Plot of $1/\eta_0^{\otimes}$ vs $1/C_i^0$.

invalidate the assessment. Nevertheless, the results of Xi et al.[20] employing a similar reactor geometry and radiation emitting source can be used for comparison purposes. The photonic efficiency obtained by Xi et al. for a DCA concentration of 5.0 mmol L^{-1} was approximately 12%, using aeroxide TiO_2 P25 as catalyst and an incident radiation flux of 50 W m^{-2}. At similar experimental conditions, we obtained a value of 11%.

(b) Influence of the Catalyst Concentration. Figure 9a presents the dimensionless concentration of DCA vs time for different TiO_2 concentrations, for $C_i^0 = 1$ mmol L^{-1}. The photocatalytic degradation increases with the catalyst loading, but when the concentration of TiO_2 surpasses 0.5 g L^{-1}, the process becomes independent of the catalyst concentration. Model predictions, calculated with eq 14, represent with good accuracy the experimental results.

The behavior of the photocatalytic process with the catalyst loading can be attributed to the catalyst absorption efficiency. The only parameter of eq 14 that depends on the catalyst concentration is ϑ_{cat}, that reaches a maximum value at a TiO_2 concentration of 0.5 g L^{-1}, as reported in Figure 7a. This effect is also evident in Figure 9b, where the experimental ratio $\zeta_0^{\otimes}/\zeta_0^{max}$ and the ratio $\vartheta_{cat}/\vartheta_{cat}^{max}$, computed with the radiation model, are plotted against the catalyst concentration. Considering that $\zeta_0^{\otimes} = \vartheta_{cat}\eta_0^{\otimes}$ and $\zeta_0^{max} = \vartheta_{cat}^{max}\eta_0^{\otimes}$, the experimental values of $\zeta_0^{\otimes}/\zeta_0^{max}$ can be used to verify the radiation model estimations of $\vartheta_{cat}/\vartheta_{cat}^{max}$.

(c) Influence of Radiation Intensity. The effect of radiation intensity on the photocatalytic degradation of DCA can be assessed by varying the incident photon flux. In the present work, this task was accomplished by changing the distance between the lamps and the reactor. Figure 10 represents the

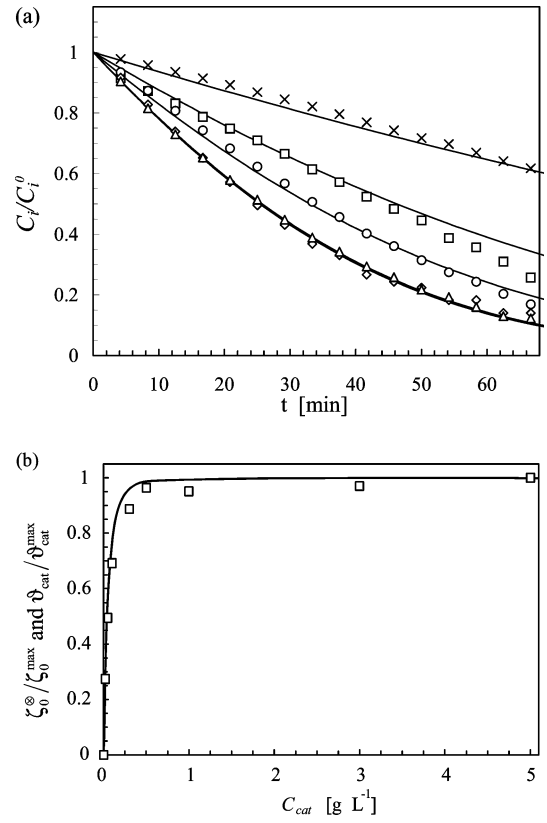

Figure 9. (a) Dimensionless DCA concentration as a function of time for different catalyst concentrations. Symbols: experimental data. Solid lines: model predictions. PBR Ib. $d_{PR} = 12.8$ mm. $C_i^0 = 1$ mmol L^{-1}. (×) $C_{cat} = 0.02$ g L^{-1}, (□) $C_{cat} = 0.05$ g L^{-1}, (○) $C_{cat} = 0.1$ g L^{-1}, (◇) $C_{cat} = 0.5$ g L^{-1}, (△) $C_{cat} = 5.0$ g L^{-1}. (b) Normalized initial OPE and normalized catalyst absorption efficiency as a function of the catalyst concentration: (□) $\zeta_0^{\otimes}/\zeta_0^{max}$. Solid line: $\vartheta_{cat}/\vartheta_{cat}^{max}$.

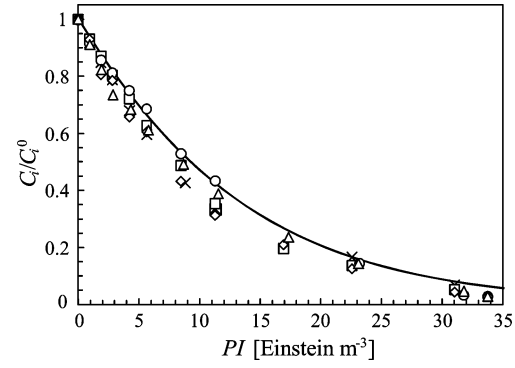

Figure 10. Dimensionless concentration of DCA as a function of the photon input (PI) for different relative photon fluxes. Symbols: experimental data. Solid line: model prediction. PBR Ib. $d_{PR} = 12.8$ mm. $C_{cat} = 0.5$ g L^{-1}. $C_i^0 = 1$ mmol L^{-1}. (×) $q_{inc}^{rel} = 0.20$, (□) $q_{inc}^{rel} = 0.49$, (○) $q_{inc}^{rel} = 0.63$, (◇) $q_{inc}^{rel} = 0.83$, (△) $q_{inc}^{rel} = 1.00$.

dimensionless concentration of DCA vs the *photon input* (PI), defined for different relative photon fluxes $q_{inc}^{rel} = q_{inc}^{\Delta\lambda}/q_{inc}^{\Delta\lambda,\otimes}$ as[9]

$$PI = \frac{A_{inc}}{\varepsilon_L V_{Sys}} q_{inc}^{\Delta\lambda} t \qquad (25)$$

The reference photon flux was $q_{inc}^{\Delta\lambda,\otimes} = 6.30 \times 10^{-5}$ Einstein m^{-2} s^{-1}. The initial DCA concentration was 1 mmol L^{-1}, and the catalyst concentration was 0.5 g L^{-1}. The DCA dimensionless concentration predicted by the L-H_{Ph} kinetics is also shown

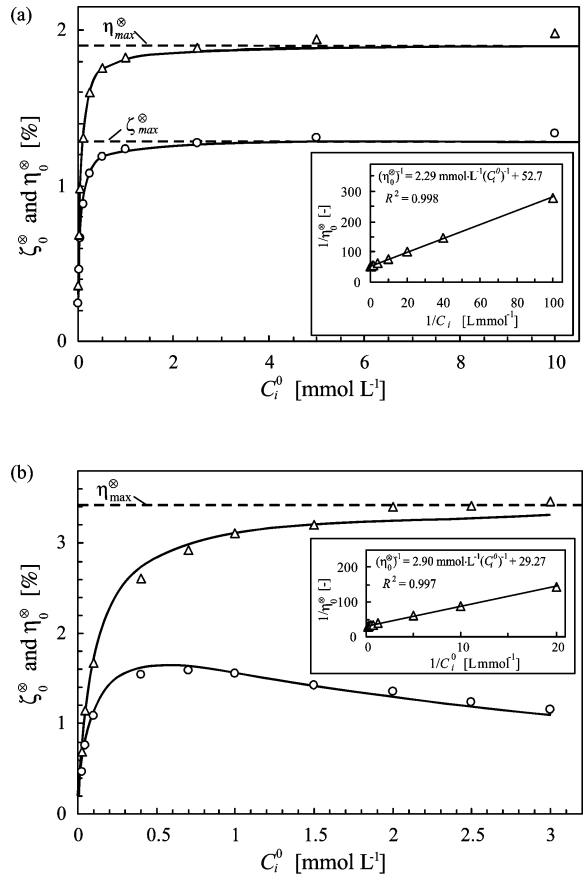

Figure 11. Reference initial OPE $\zeta_0^{\otimes}$ and reference initial removal efficiency $\eta_0^{\otimes}$ vs initial pollutant concentration. PBR Ia. $d_{PR} = 12$ mm. $C_{cat} = 5.0$ g L^{-1}. (a) Phenol. (b) 4-NP. Symbols: experimental data. Solid lines: model predictions. (△) $\eta_0^{\otimes}$, (○) $\zeta_0^{\otimes}$. (insert) Plot of $1/\eta_0^{\otimes}$ vs $1/C_i^0$.

in Figure 10. These results confirm the assumption that, under the conditions of these experiments, the photocatalytic process is independent of the photon flux ($f_q \cong 1$).

Model Pollutants: Phenol and 4-NP. (a) Influence of the Initial Pollutant Concentration. Experiments with different initial phenol and 4-NP concentrations were carried out in a PBR Ia, with an aeroxide TiO_2 P25 concentration of 5.0 g L^{-1}. The incident radiation flux was 7.07×10^{-5} Einstein m^{-2} s^{-1} and $A_{inc}/(\varepsilon_L V_{Sys}) = 91.6$ m^{-1}. Model estimations were obtained by using the L-H_{Ph}/1 kinetics (eq 21) with the parameters K, $\eta^{\otimes}_{max}$, and ϑ_{cat} computed as described previously. For phenol, the model parameters are the following: $K = 23.0$ L mmol^{-1}; $\eta^{\otimes}_{max} = 0.019$; $\vartheta_{cat} = 0.676$. In the case of 4-NP, the obtained values are the following: $K = 10.1$ L mmol^{-1}; $\eta^{\otimes}_{max} = 0.034$. The value of ϑ_{cat} depends on the 4-NP initial concentration, as was observed in Figure 6. The experimental and model values of $\zeta_0^{\otimes}$ and $\eta_0^{\otimes}$ as a function of the initial phenol and 4-NP concentrations are presented in Figure 11a and b, respectively. The inserts represent the plots $1/\eta_0^{\otimes}$ vs $1/C_i^0$ and the fitting equations to obtain the parameters K and $\eta^{\otimes}_{max}$. Model estimations show good agreement with experimental results. As predicted by the L-H_{Ph}/1 kinetics, $\eta_0^{\otimes}$ increases with the initial pollutant concentration, for both model compounds, until it reaches a maximum value. For the same C_i^0, $\zeta_0^{\otimes}$ is lower than $\eta_0^{\otimes}$ because the absorption efficiency of the catalyst is always lower than unity. In the particular case of aeroxide TiO_2 P25, ϑ_{cat} never exceeds 0.676. With respect to phenol, $\zeta_0^{\otimes}$ approaches a maximum value when the pollutant concentration increases. On the contrary, $\zeta_0^{\otimes}$ corresponding to 4-NP passes through a maximum around $C_i^0 = 0.5$ mmol L^{-1} and then decreases with

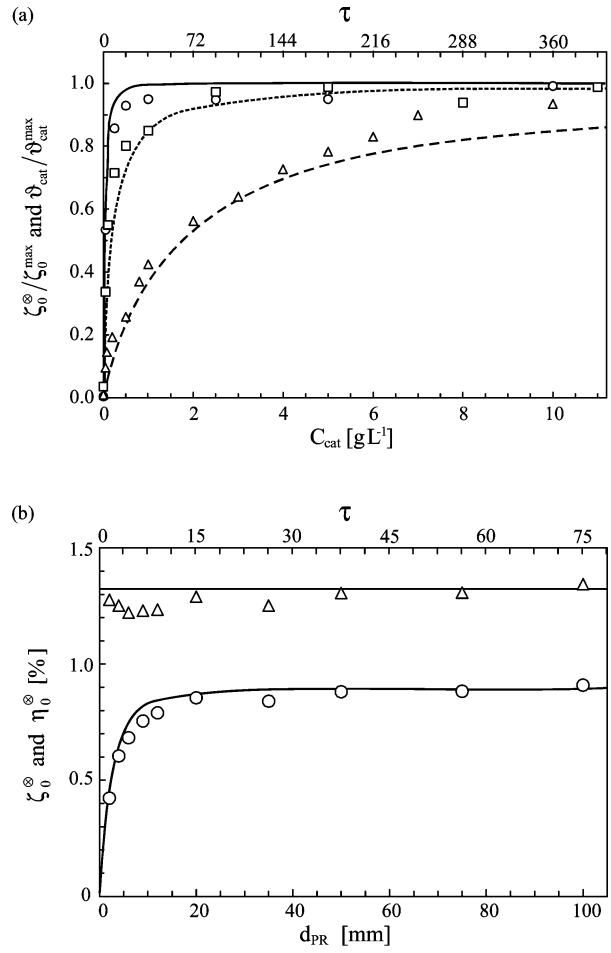

Figure 12. (a) Normalized initial OPE and normalized catalyst absorption efficiency as a function of the catalyst concentration and the optical thickness, for phenol and two concentrations of 4-NP. PBR Ia. $d_{PR} = 12$ mm. Symbols: $\zeta_0^{\otimes}/\zeta_0^{max}$. (○) C_i^0 phenol 0.1 mmol L^{-1}; (□) C_i^0 4-NP 0.1 mmol L^{-1}; (△) C_i^0 4-NP 1.0 mmol L^{-1}. Lines: $\vartheta_{cat}/\vartheta_{cat}^{max}$. (—) C_i^0 phenol 0.1 mmol L^{-1}; (•••) C_i^0 4-NP 0.1 mmol L^{-1}; (- - -) C_i^0 4-NP 1.0 mmol L^{-1}. (b) Reference initial OPE $\zeta_0^{\otimes}$ and reference initial removal efficiency $\eta_0^{\otimes}$ for phenol as a function of the reactor depth and the optical thickness. $C_{cat} = 0.25$ g L^{-1}. $C_i^0 = 0.1$ mmol L^{-1}. Symbols: experimental data. Solid lines: model predictions. (△) $\eta_0^{\otimes}$, (○) $\zeta_0^{\otimes}$.

increasing 4-NP concentration. This behavior can be attributed to the double dependency of $\zeta_0^{\otimes}$ upon the removal efficiency and the catalyst absorption efficiency: when the 4-NP concentration increases, $\eta_0^{\otimes}$ increases whereas ϑ_{cat} decreases. As a result, a maximum value of $\zeta_0^{\otimes}$ is obtained at intermediate pollutant concentrations.

(b) Influence of the Catalyst Concentration. The effect of the TiO_2 concentration on the OPE was studied in a PBR Ia for phenol at $C_i^0 = 0.1$ mmol L^{-1}, and for 4-NP at $C_i^0 = 0.1$ mmol L^{-1} and 1.0 mmol L^{-1}. Figure 12a presents the experimental ratio $\zeta_0^{\otimes}/\zeta_0^{max}$ and the theoretical ratio $\vartheta_{cat}/\vartheta_{cat}^{max}$ as a function of the catalyst concentration and the optical thickness. The catalyst absorption efficiencies calculated with the radiation model are in agreement with the OPE experimental values. Increasing the initial concentration of 4-NP the plots of both dimensionless ratios reach, as expected, the maximum value at the higher catalyst concentrations. When working with 1.0 mmol L^{-1} of 4-NP, C_{cat} must exceed 10 g L^{-1} to approximate the value of ζ_0^{max}.

(c) Influence of the Reactor Depth. The effect of the reactor depth on the OPE of phenol was studied in PBR II and PBR III. The initial phenol concentration was 0.1 mmol L^{-1}, and the TiO_2 concentration was 0.25 g L^{-1}. Model calculations take

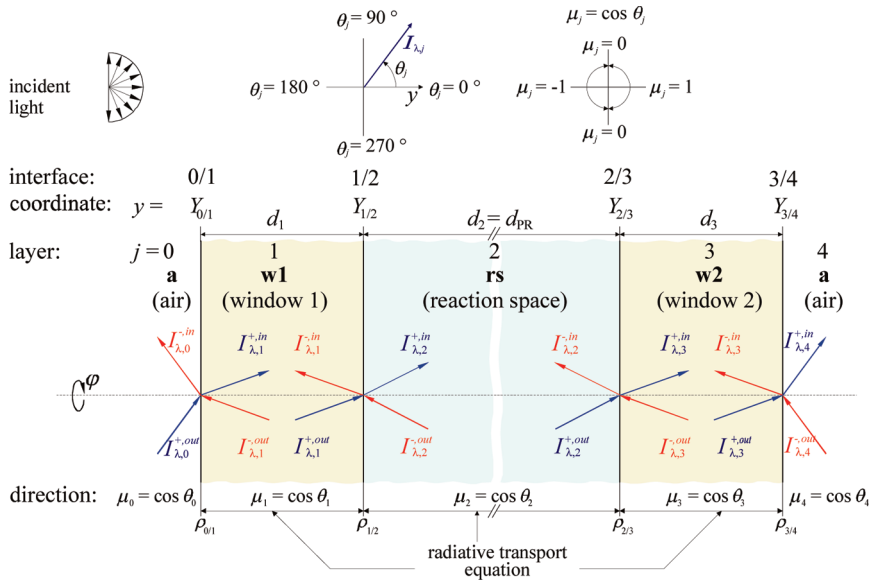

Figure A1. Description of radiation beam trajectories crossing different interfaces along the reactor depth.

into account the variations in d_{PR} through the terms $A_{inc}/(\varepsilon_L V_{Sys})$ and ϑ_{cat} (eq 21). $\zeta_0^{\otimes}$ and $\eta_0^{\otimes}$ vs the reactor depth are depicted in Figure 12b. For comparison purposes, the optical thickness τ corresponding to the reactor depth is indicated in the top x-axis.

Whereas $\eta_0^{\otimes}$ is independent of variations in the reactor depth, $\zeta_0^{\otimes}$ increases with d_{PR} and approaches a maximum value. By analyzing the plots of $\zeta_0^{\otimes}$ (or $\zeta_0^{\otimes}/\zeta_0^{\otimes,max}$) vs τ in Figure 12a and b, one can conclude that the tracing of the curve is the same when changing the catalyst concentration or the reactor depth. This observation supports the model assumption that considers $\zeta_0^{\otimes}$ directly proportional to ϑ_{cat}, which, in turn, depends on the optical thickness $\tau = \beta^*_{350nm} d_{PR} C_{cat}$ when no absorbing species are present (see Figures 7a and b). Consequently, to obtain the maximum OPE in photocatalytic plane reactors, one can either vary the catalyst concentration or the reactor depth in order to achieve the maximum ϑ_{cat}. For aeroxide TiO_2 P25, optimal conditions are obtained at $\tau = 18$.

5. Conclusions

The modeling of the photocatalytic degradation of dichloroacetic acid, phenol, and 4-nitrophenol in slurry reactors was presented. The analysis has been made in terms of the observed photocatalytic efficiency (OPE) and the removal efficiency (RE). The first parameter can be calculated from simple, observable variables such as pollutant concentration, incident photon flux, and catalyst loading. The second one requires the use of a complete radiation model for the reactor−reacting system, in terms of the apparatus configuration and the optical properties of the reactor walls, the involved reactants, and the catalyst. The radiation model was validated with radiometric measurements.

The reaction kinetics were described in terms of a "photocatalytic" Langmuir−Hinshelwood model (the L-H_{Ph} model) and a "photocatalytic" Langmuir−Hinshelwood-linear model (the L-H_{Ph}/1 model).

The observed agreement between the defined parameters and kinetic models with the experimental results was very satisfactory in all cases. The employed approach provides a simple and practical scheme to study the degradation of chemical pollutants of very different nature. The case of 4-nitrophenol permitted to investigate the effect on the catalyst absorption efficiency produced by radiation absorbing compounds. An important conclusion that can be derived from these results is that highly polluted waters, having substances that compete with titanium dioxide for absorption in the UV wavelength range, will always imply the use of high catalyst loadings.

Finally, a new type of photocatalytic, batch reactor arrangements for laboratory work, was presented. These reactors have several reaction compartments that allow one to carry out simultaneously different experiments under identical operating conditions.

Acknowledgment

The authors would like to thank to Universidad Nacional del Litoral, Consejo Nacional de Investigaciones Científicas y Técnicas, and Agencia Nacional de Promoción Científica y Tecnológica for their financial support. The technical assistance of Eng. Claudia Romani is also acknowledged. The financial contribution by SECyT (Argentina) and BMBF (Germany) with their Argentina−Germany cooperation Project (ARG 00/013) is gratefully acknowledged. G.S. and D.B. thank the European Commission for funding part of this work under the Energy, Environmental and Sustainable Development Program, contract number EVK1-CT-2000-00077.

Appendix

The RTE for a one-dimensional−one-directional radiation transport model can be expressed as

$$\mu_j \frac{\partial I^+_{\lambda,j}(y,\mu_j)}{\partial y} + \beta_{\lambda,j} I^+_{\lambda,j}(y,\mu_j) = \Sigma_{\lambda,j}(y,\mu_j) \qquad Y_{j-1/j} \le y \le Y_{j/j+1} \qquad 0 < \mu_j \le 1 \quad \text{(A.1)}$$

$$\mu_j \frac{\partial I^-_{\lambda,j}(y,\mu_j)}{\partial y} + \beta_{\lambda,j} I^-_{\lambda,j}(y,\mu_j) = \Sigma_{\lambda,j}(y,\mu_j) \qquad Y_{j-1/j} \le y \le Y_{j/j+1} \qquad -1 \le \mu_j < 0 \quad \text{(A.2)}$$

with

$$\Sigma_{\lambda,j}(y,\mu_j) = \frac{\sigma_{\lambda,j}}{2} \int_{-1}^{1} p_\lambda(\mu_j,\mu'_j) I_{\lambda,j}(y,\mu'_j)\, d\mu'_j \quad \text{(A.3)}$$

The subscript j ($j = 0, 1, ..., J$) indicates the layer (or medium) being considered. The equations presented here are generalized

for reactors with $J + 1$ layers. As illustrated in Figure A1, for the PBR, $J = 4$. The superscript out indicates the outgoing radiation at each interface, and the superscript in stands for the incoming rays. The symbol "+" represents radiation with positive μ, whereas "−" indicates radiation with negative values of μ.

The boundary condition at the external side of the front reactor window is

$$I^{+,\text{out}}_{\lambda,0}(\mu_0) = I^{+}_{\lambda,0}(Y_{0/1},\mu_0) \qquad 0 < \mu_0 \le 1 \tag{A.4}$$

Radiation coming from the lamps and arriving at $y = Y_{0/1}$ can be calculated from the experimental value of the photon flux and by considering diffuse incident radiation (intensity values are the same at all directions μ_0).

The model assumes that no radiation enters from the back window:

$$I^{-,\text{out}}_{\lambda,J}(\mu_J) = 0 \qquad -1 \le \mu_J < 0 \tag{A.5}$$

Boundary conditions for a generic layer j between the interfaces $j - 1/j$ and $j/j + 1$ are given by

$$I^{+,\text{in}}_{\lambda,j}(\mu_j) = [1 - \rho_{j-1/j}(\mu_{j-1})]\left(\frac{n_j}{n_{j-1}}\right)^2 I^{+,\text{out}}_{\lambda,j-1}(\mu_{j-1}) + \rho_{j/j-1}(-\mu_j) I^{-,\text{out}}_{\lambda,j}(-\mu_j)$$

$$0 < \mu_j \le 1 \quad \text{if } n_j < n_{j-1} \quad \text{or } \mu^{c}_{j/j-1} \le \mu_j \le 1 \text{ if } n_j > n_{j-1} \tag{A.6}$$

$$I^{+,\text{in}}_{\lambda,j}(\mu_j) = I^{-,\text{out}}_{\lambda,j}(-\mu_j) \qquad 0 < \mu_j < \mu^{c}_{j/j-1} \qquad \text{if } n_j > n_{j-1} \tag{A.7}$$

$$I^{-,\text{in}}_{\lambda,j}(\mu_j) = [1 - \rho_{j+1/j}(\mu_{j+1})]\left(\frac{n_j}{n_{j+1}}\right)^2 I^{-,\text{out}}_{\lambda,j+1}(\mu_{j+1}) + \rho_{j/j+1}(-\mu_j) I^{+,\text{out}}_{\lambda,j}(-\mu_j)$$

$$-1 \le \mu_j \le 0 \quad \text{if } n_j < n_{j+1} \quad \text{or } -1 \le \mu_j \le -\mu^{c}_{j/j+1} \text{ if } n_j > n_{j+1} \tag{A.8}$$

$$I^{-,\text{in}}_{\lambda,j}(\mu_j) = I^{+,\text{out}}_{\lambda,j}(-\mu_j) \qquad -\mu^{c}_{j/j+1} < \mu_j < 0 \qquad \text{if } n_j > n_{j+1} \tag{A.9}$$

$\mu^{c}_{j/j-1}$ is the cosine of the critical angle or angle of total reflection in j at the interface $j/j - 1$, given by $\theta^{c}_{j/j-1} = \text{sen}^{-1}(n_{j-1}/n_j)$. The term n_j represents the refractive index of the corresponding layer. Similarly, $\mu^{c}_{j/j+1}$ is defined as the cosine of $\theta^{c}_{j/j+1}$, where $\theta^{c}_{j/j+1} = \text{sen}^{-1}(n_{j+1}/n_j)$. The interface reflection coefficients ρ can be calculated by using Snell's law and Fresnel's equations. A ray entering a layer j $I^{+,\text{in}}_{\lambda,j}$ at the interface $j - 1/j$ (eq A.6) is composed by the transmitted portion of the ray coming from the adjacent layer $j - 1$ (first term of the right-hand side of eq A.6), and the reflected portion of the ray coming from the same layer j (second term of the RHS of eq A.6). The energy of the radiation is conserved in crossing the interface. Therefore, the factor $(n_j/n_{j-1})^2$ represents the gain or loss of intensity due to the change in the direction of the ray when passing into a medium of different refractive index.[15]

As shown in Figure A2, if $n_j > n_{j-1}$, layer j will receive radiation from layer $j - 1$ only at angular directions within the range $\mu^{c}_{j/j-1} \le \mu_j \le 1$. In addition, any ray incident on the interface from layer j at directions between $0 < \mu_j < \mu^{c}_{j/j-1}$ cannot enter layer $j - 1$ and is totally reflected (eq A.7). A similar analysis to the one made for eqs A.6 and A.7 can be applied

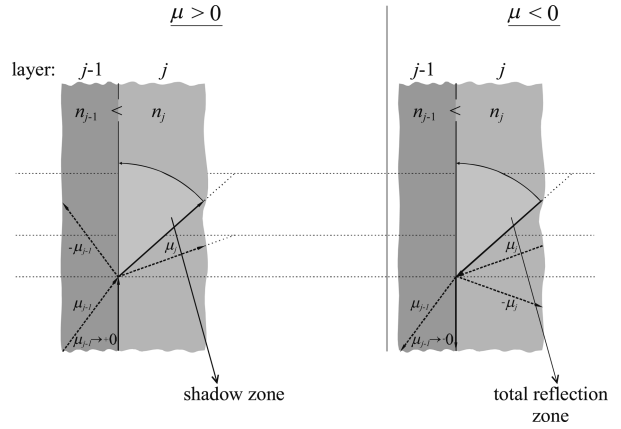

Figure A2. Description of shadow and total reflection effects produced by the radiation beam trajectory crossing different interfaces in the reactor.

for eqs A.8 and A.9. It should be noted that, strictly, n_j and ρ depend on the radiation wavelength λ, but in the present work, average values in the UV-A range are considered.

Window Plates. For layers without scattering ($j = 1$ and $j = 3$), analytical solutions of eqs A.1 and A.2 can be obtained:

$$I^{+}_{\lambda,j}(y,\mu_j) = I^{+,\text{in}}_{\lambda,j}(\mu_j)\exp\left(-\frac{\kappa_{\lambda,j}}{\mu_j}(y - Y_{j-1/j})\right) \qquad Y_{j-1/j} \le y \le Y_{j/j+1} \qquad 0 < \mu_j \le 1 \tag{A.10}$$

$$I^{-}_{\lambda,j}(y,\mu_j) = I^{-,\text{in}}_{\lambda,j}(\mu_j)\exp\left(-\frac{\kappa_{\lambda,j}}{\mu_j}(y - Y_{j/j+1})\right) \qquad Y_{j-1/j} \le y \le Y_{j/j+1} \qquad -1 \le \mu_j < 0 \tag{A.11}$$

The boundary conditions of eqs A.10 and A.11 are given by eqs A.6−A.9.

Notation

A_{inc} = area of incident radiation, m^2
C_{cat} = catalyst mass concentration, g L^{-1}
C_i = actual pollutant concentration, mmol L^{-1}
C_i^0 = initial pollutant concentration, mmol L^{-1}
d_{PR} = reactor depth, mm
$e^{\Delta\lambda}_{\text{abs}}$ = local volumetric rate of photon absorption in the $\Delta\lambda$ wavelength range, Einstein m^{-3} s^{-1}
f_q = correction function for the photon flux, dimensionless
g_λ = spectral asymmetry factor, dimensionless
I_λ = spectral radiation intensity, Einstein m^{-2} sr^{-1} s^{-1}
K = kinetic parameter, L $mmol^{-1}$
n = refractive index, dimensionless
$\underline{n}$ = unit normal vector
N_{rem} = amount of substance removed from the liquid, mol
$P^{\Delta\lambda}_{\text{inc}}$ = amount of incident photons in the $\Delta\lambda$ wavelength range, Einstein
$\text{PD}^{\otimes}$ = photon demand, Einstein m^{-3}
PI = photon input, Einstein m^{-3}
p = phase function for scattering, dimensionless
$p_{\text{HG},\lambda}$ = Henyey and Greenstein phase function, dimensionless
$q^{\Delta\lambda}_{\text{inc}}$ = incident photon flux in the $\Delta\lambda$ wavelength range, Einstein m^{-2} s^{-1}
$q^{\Delta\lambda,\otimes}_{\text{inc}}$ = reference incident photon flux in the $\Delta\lambda$ wavelength range, Einstein m^{-2} s^{-1}
$q^{\text{rel}}_{\text{inc}}$ = relative incident photon flux, dimensionless
R_{Ref} = relative reflected radiation, dimensionless
R_{Trans} = relative transmitted radiation, dimensionless
t = time, s or min

$\underline{x}$ = position vector
x, y, z = Cartesian coordinates
$V_{Sys,L}$ = liquid reactor volume, m^3
V_{Sys} = reactor volume, m^3
Greek Letters
β_λ = catalyst spectral extinction coefficient, cm^{-1}
β_λ^* = catalyst spectral specific extinction coefficient, $cm^2\ g^{-1}$
Δ = interval
ε_L = liquid hold up, dimensionless
ζ_{act}^{obs} = actual observed photonic efficiency (actual OPE), mol $Einstein^{-1}$
$\zeta^{\otimes}$ = actual OPE at reference photon flux, mol $Einstein^{-1}$
$\zeta_{max}^{\otimes}$ = maximum OPE at reference photon flux, mol $Einstein^{-1}$
$\zeta_0^{\otimes}$ = initial OPE at reference photon flux, mol $Einstein^{-1}$
ζ_0^{max} = initial OPE at ϑ_{cat}^{max}, mol $Einstein^{-1}$
η_{remov} = removal efficiency, mol $Einstein^{-1}$
$\eta_0^{\otimes}$ = initial removal efficiency at reference photon flux, mol $Einstein^{-1}$
$\eta_{max}^{\otimes}$ = maximum removal efficiency at reference photon flux, mol $Einstein^{-1}$
ϑ_{cat} = catalyst absorption efficiency, dimensionless
ϑ_{cat}^{max} = maximum catalyst absorption efficiency, dimensionless
θ = azymuthal angle, rad
θ^c = critical angle, rad
κ_λ = catalyst spectral absorption coefficient, cm^{-1}
κ_λ^* = catalyst spectral specific absorption coefficient, $cm^2\ g^{-1}$
$\kappa_{\lambda,i}^*$ = spectral molar absorption coefficient of pollutant i, L mol^{-1} cm^{-1}
λ = radiation wavelength, nm
μ = cosine of θ
μ^c = cosine of the critical angle
μ' = cosine of the scattered angle
μ^* = cosine of the angle formed by the incident and scattered rays
ρ = interface reflection coefficient, dimensionless
Σ = source function defined in eq A.3
σ_λ = catalyst spectral scattering coefficient, cm^{-1}
σ_λ^* = catalyst spectral specific scattering coefficient, $cm^2\ g^{-1}$
τ = optical thickness, dimensionless
ψ^0 = initial conditions
Ω = solid angle of radiation propagation, sr
$\underline{\Omega}$ = unit vector in the direction of radiation propagation
Special Symbols
$\langle\rangle$ = average value
$\otimes$ = reference photon flux

Literature Cited

(1) Gaya, U. I.; Abdullah, A. H. Heterogeneous Photocatalytic Degradation of Organic Contaminants over Titanium Dioxide: A Review of Fundamentals, Progress and Problems. *J. Photochem. Photobiol. C* **2008**, *9*, 1.

(2) Cabrera, M. I.; Alfano, O. M.; Cassano, A. E. Novel Reactor for Photocatalytic Kinetic Studies. *Ind. Eng. Chem. Res.* **1994**, *33*, 3031.

(3) Brandi, R. J.; Citroni, M. A.; Alfano, O. M.; Cassano, A. E. Absolute Quantum Yields in Photocatalytic Slurry Reactors. *Chem. Eng. Sci.* **2003**, *58*, 979.

(4) Camera-Roda, G; Santarelli, F; Martín, C. A. Design of Photocatalytic Reactors Made Easy by Considering the Photons as Immaterial Reactants. *Solar Energy* **2005**, *79*, 343.

(5) Li Puma, G. Dimensionless Analysis of Photocatalytic Reactors Using Suspended Solid Photocatalysts. *Chem. Eng. Res. Des.* **2005**, *83*, 820.

(6) Li Puma, G.; Brucato, A. Dimensionless Analysis of Slurry Photocatalytic Reactors Using Two-Flux And Six-Flux Radiation Absorption-Scattering Models. *Catal. Today* **2007**, *122*, 78.

(7) Satuf, M. L.; Brandi, R. J.; Cassano, A. E.; Alfano, O. M. Quantum Efficiencies of 4-Chlorophenol Photocatalytic Degradation and Mineralization in a Well-mixed Slurry Reactor. *Ind. Eng. Chem. Res.* **2007**, *46*, 43.

(8) Camera-Roda, G; Santarelli, F; Panico, M. Study and Optimization of an Annular Photocatalytic Slurry Reactor. *Photochem. Photobiol. Sci.* **2009**, *8*, 712.

(9) Sagawe, G.; Brandi, R. J.; Bahnemann, D.; Cassano, A. E. Photocatalytic Reactors for Treating Water Pollution with Solar Illumination. I: A Simplified Analysis for Batch Reactors. *Chem. Eng. Sci.* **2003**, *58*, 2587.

(10) Alfano, O. M.; Cabrera, M. I.; Cassano, A. E. Photocatalytic Reactions Involving Hydroxyl Radical Attack. I. Reaction Kinetics Formulation with Explicit Photon Absorption Effects. *J. Catal.* **1997**, *172*, 370.

(11) Bahnemann, D. W.; Hilgendorff, M.; Memming, R. Charge Carrier Dynamics at TiO_2 Particles: Reactivity of Free and Trapped Holes. *J. Phys. Chem. B* **1997**, *101*, 4265.

(12) Bahnemann, D. W.; Kholuiskaya, S. N.; Dillert, R.; Kulak, A. I.; Kokorin, A. I. Photodestruction of Dichloroacetic Acid Catalyzed by Nanosized TiO_2 Particles. *Appl. Catal., B* **2002**, *36*, 161.

(13) Zalazar, C. S.; Romero, R. L.; Martín, C. A.; Cassano, A. E. Photocatalytic Intrinsic Reaction Kinetics. I: Mineralization of Dichloroacetic Acid. *Chem. Eng. Sci.* **2005**, *60*, 5240.

(14) Satuf, M. L.; Brandi, R. J.; Cassano, A. E.; Alfano, O. M. Experimental Method to Evaluate the Optical Properties of Aqueous Titanium Dioxide Suspensions. *Ind. Eng. Chem. Res.* **2005**, *44*, 6643.

(15) Siegel, R.; Howell, J. R. *Thermal Radiation Heat Transfer*, 4th ed.; Hemisphere Publishing Corp.: Bristol, PA, 2002.

(16) Matthews, R. W. Photooxidation of Organic Impurities in Water Using Thin Films of Titanium Dioxide. *J. Phys. Chem.* **1987**, *91*, 3328.

(17) Matthews, R. W. Photocatalytic Oxidation and Adsorption of Methylene Blue on Thin Films of Near-Ultraviolet-Illuminated TiO_2. *J. Chem. Soc.* **1989**, *85*, 1291.

(18) Özişik, M. N. *Radiative Transfer and Interactions with Conduction and Convection*; Wiley: New York, 1973.

(19) Duderstadt, J. J.; Martin, R. *Transport Theory*; Wiley: New York, 1979.

(20) Xi, W.; Geissen, S. U.; Vogelpohl, A. Solar Detoxification of Wastewater in a Novel Aerated Cascade Photoreactor. *Water Sci. Technol.* **2001**, *44*, 237.

Received for review November 5, 2009
Revised manuscript received February 15, 2010
Accepted February 18, 2010

IE901753K